Unravelling the Physicochemical Properties of Poly(2-*n*-propyl-2-oxazoline), a Promising Pharmaceutical Excipient

Authors: Tom Konings[1], Bart Goderis[2], Richard Hoogenboom[3], Wouter Marchal[4], Guy Van den Mooter[1]*

Affiliations

1. Drug Delivery and Disposition, KU Leuven, Department of Pharmaceutical and Pharmacological Sciences, Campus Gasthuisberg ON2, Herestraat 49 b921, 3000 Leuven, Belgium.
2. Polymer Chemistry and Materials, KU Leuven, Celestijnenlaan 200F, B-3001 Leuven, Belgium.
3. Supramolecular Chemistry Group, Centre of Macromolecular Chemistry (CMaC), Department of Organic and Macromolecular Chemistry, Ghent University, Krijgslaan 281-S4, B-9000 Ghent, Belgium.
4. Analytical and Circular Chemistry, Institute for Materials Research (imo-imomec), Hasselt University, Agoralaan Building D, 3590 Diepenbeek, Belgium.

This graphic is for Table of Contents use only

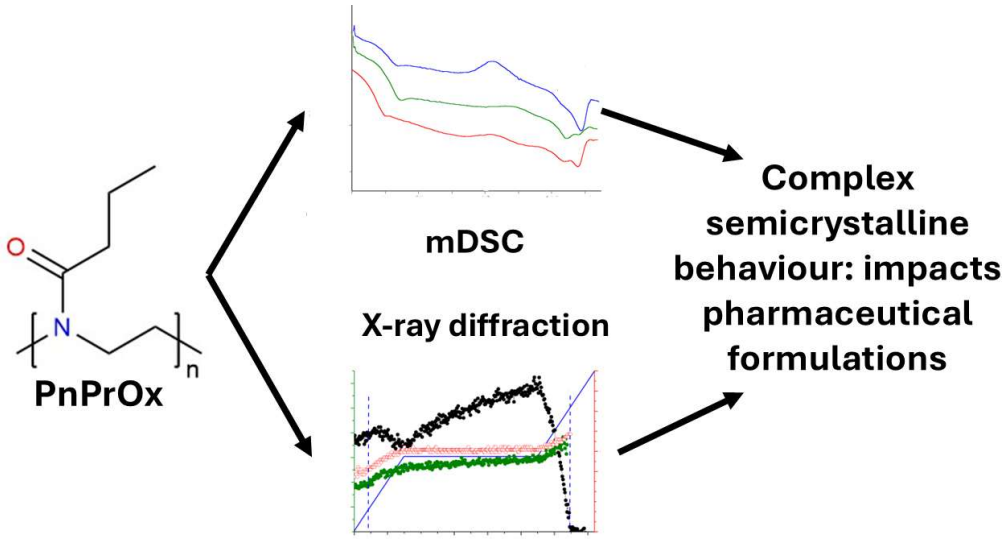

Keywords

Polymer melting, Poly(2-alkyl/aryl-2-oxazoline)s, modulated differential scanning calorimetry, X-ray diffraction, excipient characterization, semi-crystalline polymer

Konings, Tom; Goderis, Bart; Hoogenboom, Richard; MARCHAL, Wouter & van den Mooter, Guy (2025) Unraveling the Physicochemical Properties of Poly(2-n-propyl-2-oxazoline), a Promising Pharmaceutical Excipient. In: Macromolecules, 58 (16) , p. 8727 -8740.
DOI: 10.1021/acs.macromol.5c00794

Abbreviations

PAOx	Poly(2-alkyl/aryl-2-oxazoline)s
PnPrOx	Poly(2-*n*-propyl-2-oxazoline)
Đ	Dispersity
T_{Cp}	Cloud point temperature
T_g	Glass transition temperature
T_c	Crystallisation temperature
PEtOx	Poly(2-ethyl-2-oxazoline)
PsecBuOx	Poly(2-*sec*-butyl-2-oxazoline)
ASD	Amorphous solid dispersion
Mn	Number average molecular mass
T_m	Melting temperature
PiPrOx	Poly(2-*i*sopropyl-2-oxazoline)
LCST	Lower critical solution temperature
mDSC	Modulated differential scanning calorimetry
XRPD	X-ray powder diffraction
SAXS	Small-angle X-ray scattering
WAXS	Wide-angle X-ray scattering
q	Scattering vector

Abstract

Poly(2-alkyl/aryl-2-oxazoline)s (PAOx) are biocompatible polymers that are increasingly being applied in the biomedical field. Understanding their properties is crucial to rationally apply them in said field. Despite this increasing interest, many fundamental properties of PAOx, such as the semi-crystalline nature of poly(2-*n*-propyl-2-oxazoline) (PnPrOx) have not been fully elucidated yet, especially for higher molar mass polymers. In the present work, the crystallinity of PnPrOx was studied using modulated DSC as well as small-angle and wide-angle X-ray scattering. This study reveals that high molar mass PnPrOx show a much richer phase behaviour than their amorphous low molar mass counterparts. For instance, aqueous solutions turn cloudy upon prolonged exposure to high temperature due to crystallisation of the phase separated high polymer concentration mesoglobules. Moreover, dry solid samples display polymorphisms as well as a multiple melting behaviour due to the presence of different crystal sizes and overlapping crystallisation and melting events. This work suggests that additional research into the semi-crystalline properties of other higher molar mass PAOx might be required to evaluate whether they have similar behaviour to higher molar mass PnPrOx. Additionally, the results presented in this manuscript will allow for the rational development and design of pharmaceutical formulations containing PAOx, as it elucidates some of their fundamental properties.

1 Introduction

Poly(2-alkyl/aryl-2-oxazoline)s (PAOx) are an emerging class of biocompatible polymers for biomedical applications. (1–3) The structures of several PAOx that have been studied as pharmaceutical excipients are shown in Figure 1. (4) PAOx offer several advantages when compared to other commonly used pharmaceutical polymer excipients, such as ethyl cellulose or poly(vinyl pyrrolidone). (5) Firstly, they can be synthesized with a low dispersity (Đ) via a living cationic ring opening polymerization reaction, making them suitable for a wide range of formulations. (6,7) Moreover, polymers with different side chains and, thus, different physicochemical properties can be readily synthesized. Possible side chains include linear, branched, or cyclic alkyl substituents, chains with aromatic groups, chains containing nitrogen functional groups such as protected amines or amides, or even fully fluorinated alkyl chains, to list a few. (2,6) This large diversity in side-chains provides tuneability of PAOx properties, including design of smart polymers. (1,8,9) It has been demonstrated that the lower critical solution temperature behaviour in water and the cloud point temperatures, T_{cp}, as well as the glass transition temperature, T_g, and crystallisation temperature, T_c, in the pure solid state, depend on the polymer side-chain composition. (3,10)

Figure 1. The chemical structures of several PAOx that have been reported as pharmaceutical excipients: poly(2-ethyl-2-oxazoline) (PEtOx), poly(2-n-propyl-2-oxazoline) (PnPrOx), and poly(2-sec-butyl-2-oxazoline) (PsecBuOx).

This versatility of PAOx has inspired their evaluation for numerous biomedical applications, including nanoparticle drug delivery, matrix delivery systems, amorphous solid dispersions, antifouling coatings, and hydrogels, among others. (11,12) For a review regarding current emerging trends, the reader is referred to a paper by Hoogenboom. (13) The number of potential applications of PAOx in nanoparticle drug delivery systems is particularly impressive and was reviewed by Wilson *et al.* (12) Possible applications in this field make use of PAOx in the form of microbeads, capsules, vesicles, micelles, stars, dendrimers, and nanogels.

Additionally, Keßler *et al.* (14) recently applied PAOx in the formulation of amorphous solid dispersions with indomethacin. Moreover, poly(2-ethyl-2-oxazoline) (PEtOx) was compared to several commonly used polymers for the formulation of amorphous solid dispersions (ASDs) by Boel *et al*, who indicated that PEtOx could maintain drug supersaturation. (15) PAOx were also applied to stabilize nanoparticles by Ramsey *et al.*, who used them to stabilize remdesivir for aerosol treatment of COVID-19. (16) Samaro *et al.* formulated tablets with a high drug loading by using several PAOx, including PnPrOx, as a sustained release matrix system. (17) The use of PnPrOx as a sustained release matrix, combined with the ability of the structurally similar PEtOx to stabilize ASDs, suggests that PnPrOx may also be suitable for formulating ASDs with a sustained release profile. Sustained release is a commonly used oral drug delivery strategy that aims at stabilizing plasma concentration levels of drugs, resulting in less toxicity and an improved therapeutic effect. Applying this concept for ASDs has gained a lot of interest recently (18,19), and the hydrophobicity of PnPrOx makes it a good candidate for this application.

Knowledge of the thermal properties of PAOx is crucial for fully controlling and understanding the applications discussed above. Previously, it was reported that all PAOx with linear alkyl side chains, starting from *n*-butyl, are semi-crystalline. (24) However, there is also some evidence for crystallisation from solution for poly(2-methyl-2-oxazoline) and high molar mass (500 kg/mol) PEtOx. (25,26) There is some controversy in the literature on the crystallizability of PnPrOx, although the interesting properties of poly(2-propyl-2-oxazoline) have attracted a lot of attention over the past years. (4,10,28–31) In fact,

the monomer on which this polymer is based, has two structural isomers, namely 2-*n*-propyl-2-oxazoline and 2-isopropyl-2-oxazoline. After polymerization, these result in poly(2-*n*-propyl-2-oxazoline) (PnPrOx) and in poly(2-isopropyl-2-oxazoline) (PiPrOx). (10) Additionally, poly(2-cyclopropyl-2-oxazoline) has also been reported as related amorphous polymer structure. (32) One of the first papers about PPrOx dates from the 1960s (31) and reported that both PnPrOx and PiPrOx are semi-crystalline. However, PnPrOx has also been reported to be completely amorphous in subsequent literature, especially for shorter polymers. (33) Oleszko-Torbus *et al.* more recently confirmed the semi-crystalline nature of PnPrOx with a M_n of 8.7 kg/mol and Đ of 1.03. (10) In their study, they observed a single melting peak for PnPrOx in the 120-140 °C range, but after annealing the sample at 90 °C, they found a double melting peak in the range of 100-140 °C. (10) Later, Everaerts *et al.* also noticed the semi-crystalline character of PnPrOx with a M_n of 49.6 kg/mol and a Đ of 1.05 while studying the behaviour of PnPrOx in amorphous solid dispersions. (4) They also noticed the double melting peak. Strikingly, their peaks were not at the same temperatures when compared to the Oleszko-Torbus paper, indicating potential molar mass effects, kinetic effects, or the formation of different crystalline phases.

Whereas the glass transition temperature, T_g, is heavily affected, the melting temperature (T_m) is only slightly influenced by the nature of the side chain for PAOx, and it is located around 150 °C. (3,4) However, it can change drastically when the side chain is not linear, such as for poly(2-cycloalkyl-2-oxazoline)s, which have melting points of 240 °C - 300 °C. (27) To the best of our knowledge, there is no mention of semicrystallinity occurring in PsecBuOx in literature, and it appears to be completely amorphous in the reported thermograms from Differential Scanning Calorimetry (DSC) (4).Many polymers are subject to a lower critical solution temperature (LCST) in water. This means that they are soluble up to a certain temperature but precipitate out when the temperature is equal to the T_{Cp}. This is accompanied by a “coil to globule transition”. When in solution, the polymer is present as a hydrated coil, ensuring that interactions between the side chains and water are maximized. However, after exceeding the T_{Cp}, the polymer forms a globule to maximize the interactions which is itself driven by entropic dehydration. This transition is, in theory, reversible, and lowering the temperature should

result in the polymer being soluble again. However, if the polymer is annealed above its T_{Cp} for a sufficiently long time, crystallisation can occur. These crystals remain insoluble upon cooling, by which the cloud point transition is no longer reversible.

The irreversible precipitation from solution explained above has been observed for PAOx with methyl, ethyl, isobutyl, and nonyl side chains. (25,26,34) Additionally, Demirel *et al.* reported in 2007 that PiPrOx could also crystallize from aqueous solution when kept above its T_{Cp} for an extended time. (30) The exact mechanism behind this phenomenon is still subject to discussion, but it only occurs when the solution is kept above its T_{Cp}, meaning that the phase separation is critical. (28) Using molecular orbital calculations combined with vibrational spectroscopy, Katsumoto *et al.* (35) gave further explanation for the changes that occur upon crystallisation of PiPrOx when annealed above its T_{Cp} in aqueous solution. Aside from macroscopic phase separation, they described that the PiPrOx chains dehydrate and subsequently undergo a conformational change. This then results in a crystallizable all-trans configuration that can only be reversed by melting the polymer crystals. Cooling the solution below the T_{Cp} does not result in PiPrOx redissolution as they remain stable in the all-trans polymer crystals.

In this study, we investigated previously unexplored thermal properties of PnPrOx with different molar mass in the solid state as well as in aqueous solution. Understanding these properties is crucial to fully grasp the potential of this polymer as a pharmaceutical excipient. Hence, we provide novel insights regarding the semi-crystalline nature of PnPrOx using modulated differential scanning calorimetry (mDSC), temperature resolved X-ray powder diffraction (XRPD), as well as synchrotron small and wide-angle X-ray scattering. We also confirmed the completely amorphous nature of PEtOx in the absence of solvent and of PsecBuOx.

2 Materials and methods

2.1 Materials

The syntheses of PnPrOx (with Mn 50 kg/mol and Đ ≤ 1.25), PEtOx (with Mn 100 kg/mol and Đ ≤ 1.3, respectively), and PsecBuOx (with Mn 44.6 kg/mol and Đ = 1.07) have been reported previously. (17) PnPrOx (with Mn 23 and 11 kg/mol, and Đ ≤ 1.25) and PEtOx (with Mn 50 kg/mol and Đ ≤ 1.25) were obtained from Avroxa BV (Zwijnaarde, Belgium).

Phosphorous pentoxide (98+ %, ACS) was acquired from Thermo scientific® (Dreieich, Germany). Purified water (18.2 MΩ) was obtained from a Purelab® flex water purification system (Tienen, Belgium). Acetone (>99 %) was acquired from VWR® (Rosny-sous-Bois-Cedex, France).

2.2 Freeze drying

To ensure that the thermal history of PnPrOx and PEtOx would not influence the analyses, the polymers were first redissolved and freeze dried using an alpha 2.4-LSC plus® freeze dryer (Martin Christ®, Osterode am Harz, Germany). The protocol is described in the supplementary information (S1). The residual water content was determined using thermogravimetric analysis to be 1.9% m/m for PnPrOx, and 2.0% m/m for PEtOx and is further described in S1.

Redissolution and freeze drying was not possible for PsecBuOx since it is water insoluble. It also is not hygroscopic, so performing this step was not relevant for this polymer. The remaining solvent content for this polymer was determined by TGA to be 5.3% m/m.

2.3 Modulated differential scanning calorimetry

Modulated differential scanning calorimetry (mDSC) was conducted using Discovery 2500® and Q2000® mDSCs, both equipped with RCS90 refrigerated cooling systems (TA Instruments®, Leatherhead, U.K.). Dry nitrogen with a 50 mL/min flow rate was used as a purge gas. Temperature and enthalpy calibrations were performed with indium at a heating rate of 2 °C/min. In addition, temperature calibrations (for 2 °C/min) were also performed for octadecane and tin. Finally, the equipment was also calibrated for heat capacity using a heating rate of 2 °C/min with sapphire. No calibrations were performed for the other heating rates described in this paper, but an indium reference was analysed using heating rates of 1 °C/min and 10 °C/min for a qualitative analysis.

Samples of 4.5 to 5.5 mg were analysed in duplicate or triplicate with two or three heating runs depending on the experiment. The lids of the standard not hermetic aluminium mDSC pans were perforated using a needle for all experiments on PnPrOx, resulting in two holes of approximately 1 mm in diameter. The reader is referred to sections S3 and S4 in the supporting information for more information on the effects observed when perforated mDSC pan lids were used. Perforating the lid was done to facilitate the moisture escape, which presumably already started upon loading the sample in the dry nitrogen atmosphere of the mDSC. As a result, perforation led to a reduction of the moisture evaporation peak in the actual experiments and a clearer T_g.

For all measurements, the modulation amplitude was set at 0.212 °C and the period was set at 40 s, resulting in at least 4 modulations per thermal transition. Samples were analysed between -10 °C and 160 °C for the first heating run and between 10 °C and 160 °C for subsequent heating runs. Every heating run was preceded by a one-minute isothermal step. Different heating rates, cooling rates, and annealing temperatures were used to assess PnPrOx crystallinity.

In a first set of experiments, heating and cooling rates were varied (see Figure 2a and Figure 2b, respectively). Firstly, heating rates of either 1 °C/min or 2 °C/min were used, after the sample was cooled from the melt at 160 °C at an average rate of 47 °C/min (Figure 2a). This nominal rate is based

on the time it took the mDSC to decrease the temperature from 160 °C to the starting temperature. Then, controlled cooling rates of 2 °C/min and 5 °C/min were used (Figure 2b), but the heating rate was always kept constant at 2 °C/min. At the end of these experiments, the samples were cooled at 47 °C/min and stored at room temperature. After one week storage, the samples were subjected to exactly the same mDSC experiments once again.

Since PEtOx and PsecBuOx were confirmed to be fully amorphous under the conditions studied in this manuscript (see results), they were only subjected to a heating rate of 2 °C/min after having been cooled at an average rate of 47 °C/min. As for PnPrOx, the effect of perforating pan lids was studied for these polymers as well.

A second set of experiments (see Figure 2c) studied the effect of high temperature annealing time combined with different heating rates. First, samples were melted by heating to 160 °C, followed by cooling to 20 °C at the average maximum rate of 47 °C/min. This was followed by annealing the samples at 105 °C for two hours (the heating rate from 20 °C to 105 °C was always 2 °C/min). 105 °C was chosen as the annealing temperature to ensure the samples would be maximally crystalline. From the mDSC data in results section 3.2.2, one can indeed conclude that this temperature is sufficient to induce crystallisation, independent of sample history. Following this, the samples were cooled to 20 °C at 2 °C/min before heating again to 160 °C at 1 °C/min, 2 °C/min or 10 °C/min depending on the experiment. This experiment was also done with lower M_n PnPrOx (11 and 23 kg/mol), to study the effect of molar mass on semicrystalline behaviour. Furthermore, this experiment was also conducted on PEtOx and PsecBuOx to confirm their amorphous nature under these conditions.

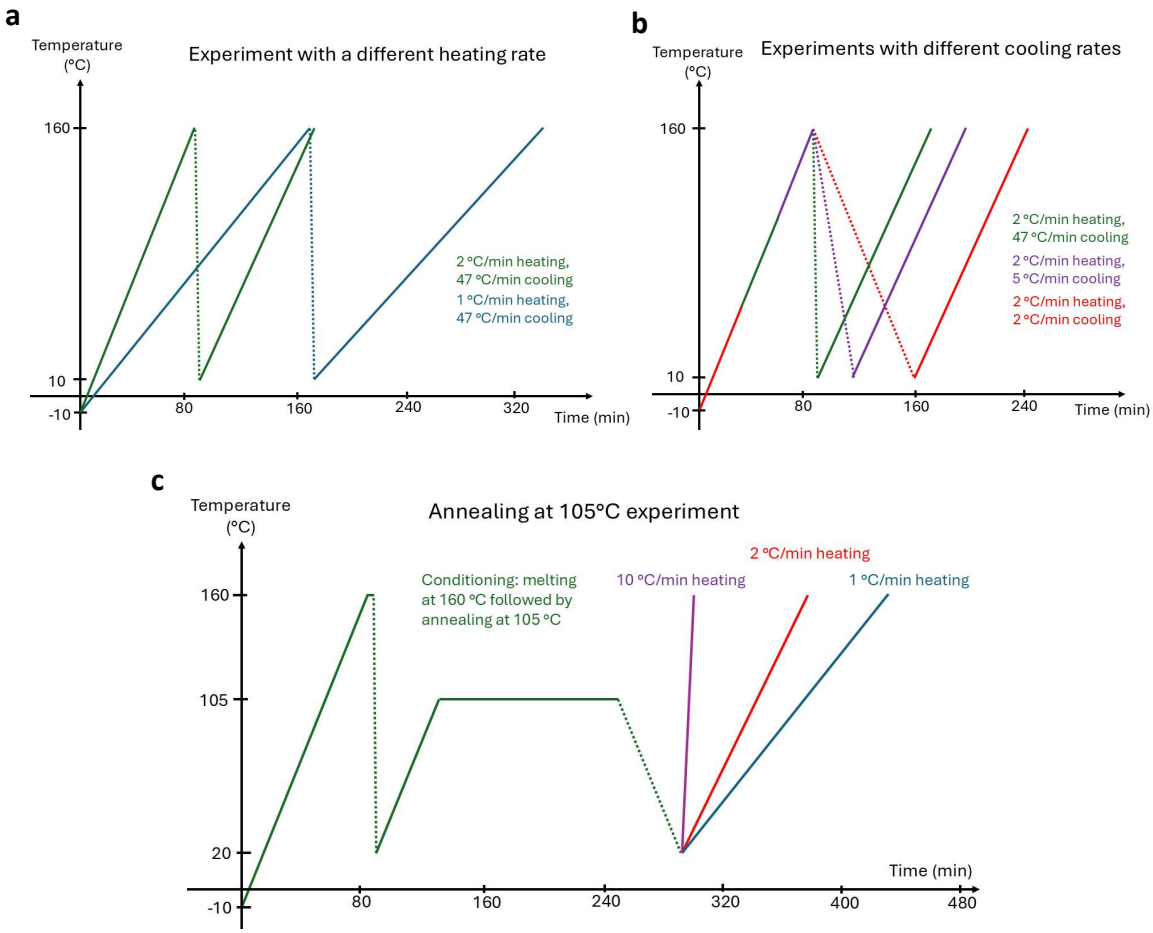

Figure 2. Summary of the different heating cycles and parameters used in the mDSC experiments

Finally, two samples were conditioned outside the mDSC and analysed using a simple protocol. One sample was rendered fully amorphous by melting it at 160 °C and keeping it at that temperature for five minutes, followed by flash cooling with liquid nitrogen. This sample was then kept in an oven at 60 °C for one week and subsequently analysed by heating to 160 °C at 2 °C/min, preceded by a 60 minute isothermal step at 30 °C. The reason for performing the annealing at 60 °C was to study the effect of this longer annealing time at lower temperature on the double melting peak (see results). The other sample was obtained by crystallisation from aqueous solution (see point 4 in methods) and analysed using the same parameters. This experiment was performed to confirm whether the irreversible transition (crystallisation) that was observed for PiPrOx solutions also occurred in PnPrOx solutions kept above the T_{cp}.

TRIOS® software version 5.2 (TA Instruments®, Leatherhead, U.K.) was used for data analysis. T_g midpoints were calculated by determining the temperature at half the step height. The curves were displaced vertically for better comparison in overlay figures.

2.4 Crystallisation from aqueous solution

Aqueous PnPrOx solutions 10% (m/V) were prepared using purified water and stored above their T_{Cp} (approximately 25 °C) (36,37) at 61 °C (this exact temperature determined using a thermocouple). After four days, the solution was stored in the refrigerator (between 4 °C and 8 °C) overnight. Precipitated material was then removed from the beaker and subsequently analysed using mDSC and XRPD. It must be noted that the sample was not dried to avoid any further crystallisation due to water evaporation. The residual water content, determined by thermogravimetric analysis, was 28% m/m (supplementary information, S2), leading to an underestimation of the normalized enthalpy of fusion. An isothermal of 60 minutes at 30 °C was performed during mDSC analyses to remove the large water evaporation endotherm.

2.5 Small-angle and wide-angle X-ray scattering

Time-resolved synchrotron small-angle (SAXS) and wide-angle X-ray scattering (WAXS) experiments were performed at BM26, the Belgian beam line at the European Synchrotron Radiation Facility (ESRF) in Grenoble, France using an X-ray wavelength λ of 1.03 Å. The intensities were collected simultaneously on a Pilatus 1M detector after an evacuated tube for SAXS and a Pilatus 300k detector close to the sample for WAXS. The scattering angles were calibrated against α-alumina and silver behenate standards and the isotropic powder patterns were azimuthally averaged using the ConeX software. (38) The one dimensional data were corrected for the scattering of an empty sample holder, taking the sample transmission into account as derived from the transmitted primary beam intensity

measured by a photodiode downstream from the sample. Intensities were normalized to the intensity of the incoming beam, measured by an ionization chamber upstream from the sample. Measured intensities are presented as function of the modulus of the scattering vector q, with $q = \frac{(4\pi\ sin\theta)}{\lambda}$ and θ being half the scattering angle.

Before performing the SAXS/WAXS measurements, all samples were heated at 30 °C/min to 160 °C, kept there for 5 min to ensure that all crystals had melted and subsequently cooled at 1 °C/min to 20 °C using a DSC. The samples were kept in the standard non-hermetic aluminium DSC pans and placed in a TMS 600® hot stage (Linkam Scientific Instruments®, Surrey, UK) for temperature control during the SAXS/WAXS measurements. Liquid nitrogen was used for cooling.

Two SAXS/WAXS setups were used. The first setup consisted of subjecting the sample to a 10 °C/min heating run from 20 °C to 180 °C, interrupted by a 20 min annealing step at 95 °C. The q range was $0.006 < q < 0.38\ \text{Å}^{-1}$ for SAXS (detector placed 3 m from sample) and $0.64 < q < 2.21\ \text{Å}^{-1}$ for WAXS. The minimal SAXS q-value of 0.006 means that d-spacings up to 100 nm should be accurately detected. SAXS and WAXS patterns were taken every 6 s. Only the WAXS data was analyzed for this setup, as the SAXS data in the mentioned q range did not have useful information except for some small changes at the highest q-values, suggesting that information was hidden in the blind region between SAXS and WAXS. This region was explored in the second setup. It cannot be excluded that useful information is also hidden behind the beam stop at low q-values. This region was not further explored.

The second setup consisted of static measurements at 20 °C. The SAXS range was $0.013 < q < 0.76\ \text{Å}^{-1}$ (detector placed 1.5 m from the sample), and the WAXS range was $0.64 < q < 2.21\ \text{Å}^{-1}$, ensuring overlap between the SAXS and WAXS ranges. A sample was first conditioned in an external Mettler hot stage by cooling at 1 °C/min from 180 °C to 20 °C and statically measured at that temperature by SAXS/WAXS. The same sample was then heated at 10 °C/min to 95 °C and annealed

there for 20 min. After cooling back to 20 °C at 10 °C/min (all using an external Mettler® hot stage) the sample was measured a second time by SAXS/WAXS.

2.6 X-ray powder diffraction (XRPD)

An X'pert PRO diffractometer® (PANalytical®, Almelo, The Netherlands) with a Cu tube (Kαλ = 1.5418 Å) and a generator set-up at 45 kV and 40 mA was used in transmission mode at room temperature to conduct XRPD measurements. All scans were performed between 4° and 40° 2θ ($0.284 < q < 2.788\ \text{Å}^{-1}$) with a 400 s counting time and a 0.0167° step size. Diffractograms of PnPrOx at different temperatures were collected using an Anton Paar® (Graz, Austria) TCU 100® temperature control unit. Prior to the start of the analysis, the PnPrOx sample was heated to 180 °C, which was followed by a 5-minute isothermal and then cooling to room temperature at 10 °C/min. No higher cooling rate could be set using this instrument. Data were collected for ca. 2 hours at 25 °C increments from 50 to 175 °C. The heating rate in between the data collection isotherms was 2 °C/min. OriginPro® (version 8.5.0 SR1, OriginLab®, Northampton, USA) was used for data treatment and analysis. A fast Fourier transform filter was applied to remove noise (15 points).

3 Results

3.1 Thermal behaviour of PEtOx and PsecBuOx

First of all, perforating mDSC pan lids has some interesting effects (supplementary information section S3). It results in a lower moisture or solvent evaporation temperature (PsecBuOx) and enthalpy (PEtOx and PsecBuOx). Moreover, it results in the T_g occurring at a temperature that is 8.4 °C higher for PEtOx. The significance of this is discussed in more detail in supplementary information section S4. In summary, it can be useful to perforate mDSC pans when removing all solvent is difficult, which can result in interpretation issues regarding the mDSC analysis (in ASDs for example). Another option would be to perform a second heating run, but this completely alters the thermal history of the sample.

The mDSC thermograms obtained when heating PEtOx (50 kg/mol and 100 kg/mol) and PsecBuOx at different heating rates after annealing for two hours at 105 °C are shown in the supplementary information (section S5). Interestingly, these thermograms show none of the features that can be observed on the thermogram of PnPrOx (Figure 5). No crystallisation or melting transitions are observed at all. The only thermal event that can be observed is a T_g of 70.3 (± 0.5) °C for PEtOx 50 kg/mol, a T_g of 69.6 (± 0.2) °C for PEtOx 100 kg/mol, and a T_g of 59.0 (± 0.8) °C for PsecBuOx 50 kg/mol.

3.2 Thermal behaviour of PnPrOx

3.2.1 Temperature-resolved XRPD measurements

Figure 3 shows XRPD diffractograms obtained over the course of a temperature-resolved measurement of PnPrOx (50 kg/mol) that was melted at 180 °C and cooled back to room temperature at 10 °C/min. The first diffractogram at 50 °C suggest that the material was fully XRPD-amorphous at this temperature. Evidence that crystallisation is occurring appears at 75 °C. The peaks then increased in

intensity to a maximum at 125 °C. From 150 °C onward, melting occurs, as evidenced by the decreasing reflections. The sample is fully melted at 175 °C. The peak at ca. $q = 2.0\ \text{Å}^{-1}$ is most likely an impurity from the synthesis. It might correspond to the (111) lattice plane of pure silicon. (39)

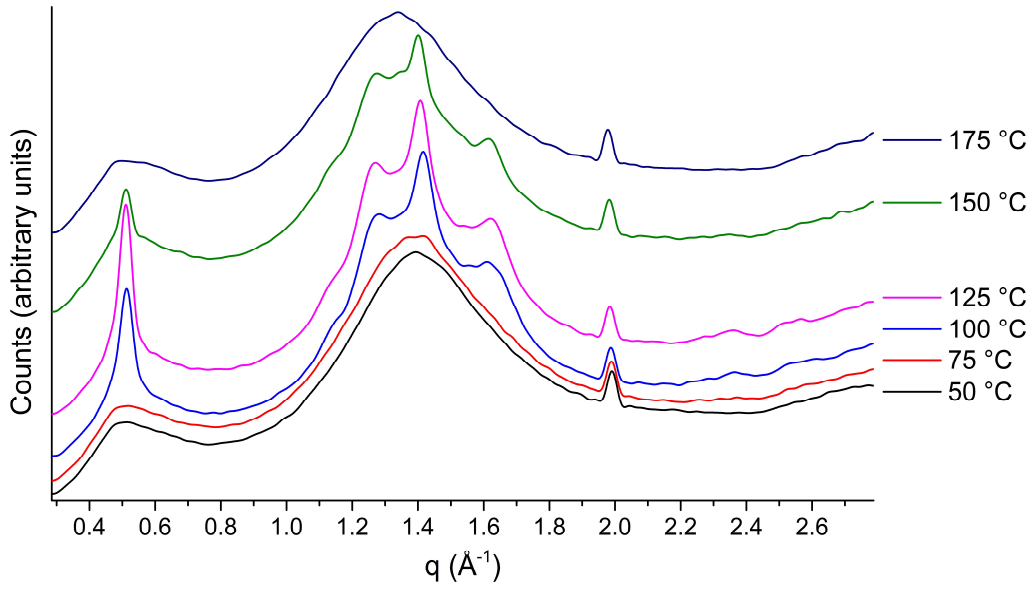

Figure 3. XRPD diffractograms of PnPrOx 50 kg/mol obtained during heating over the course of a temperature-controlled experiment.

This experiment shows that PnPrOx started to crystallize when heated above the T_g (which was determined to be 43 °C in the mDSC measurements shown later), which is so-called cold crystallisation, and has a T_m at around 150 °C. There seemed to be no solid/solid phase transitions as only one polymorph was observed. It must be said that this experiment had an important limitation, namely that each measurement took two hours. This means that the sample annealed at each temperature while it was being measured, complicating the direct comparison with mDSC results.

Synchrotron WAXS was used as a complementary technique to study the thermal behaviour of PnPrOx and to confirm the abovementioned results. Figure 4a shows the evolution of the scattering intensity with respect to time and in function of the scattering vector. The interpretation is the same as for Figure 3, but in this case, all crystals disappeared at ca. 143 °C.

Figure 4b shows several variables measured at the strongest reflection, which occurs at around $q = 1.45\ \text{Å}^{-1}$ (see Figure 3). First, it seems that the material crystallises when heated above the T_g, as evidenced by an increase in the peak intensity (black data in Figure 4b), but that this is immediately followed by a melting event upon further heating. After this first melting event, crystallisation occurred once more during the annealing step at 95 °C, followed by melting as soon as heating was continued.

Aside from crystallisation and melting, other phenomena can be observed in the WAXS data. There was some thermal expansion as evident from the increase in d-values along the heating run. On top of this, the average crystal size grew during the heating steps as well as during the isothermal step. This average crystal size growth was present even during the final melting process, as shown by the increasing Scherrer crystal size while the peak intensity was decreasing. Based on this data, the reason for this perceived average crystal growth could be the elimination of the smallest crystals, leading to an average size increase, the growth of larger crystals that have not melted yet, or a combination of these two factors.

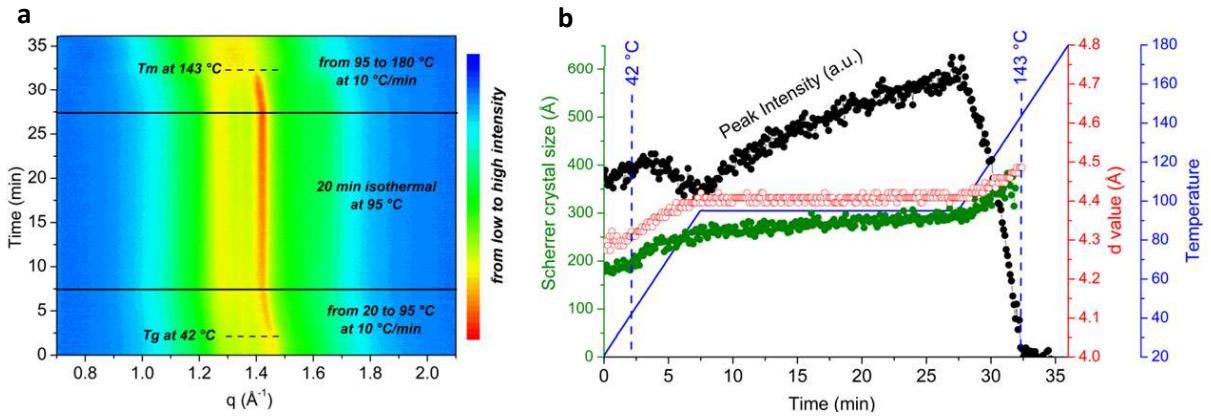

Figure 4. (a) top viewed and color coded time dependent WAXS patterns of PnPrOx 50 kg/mol as a function of the modulus of the scattering vector while heating with an intermittent 20 min annealing step at 95 °C. (b) Analysis of the strongest reflection in the WAXS range, separated from the amorphous halo using a straight sector. Scherrer crystal size, peak intensity, and d-value are shown as a function of time (and hence, temperature).

The mDSC thermogram obtained when heating the redissolved and freeze dried PnPrOx sample (50 kg/mol) as such at 2 °C/min is displayed in Figure 5, revealing a T_g of 43.5 °C (± 0.6 °C), determined on

the reversing heat flow. Figure 5 is consistent with the synchrotron WAXS data, i.e., the sample started to crystallize above the T_g for both the first and second heating run, followed by a small melting endotherm (2 and 2'), further crystallisation (3 and 3'), and a final melting event or events (4 and 4'). It is intriguing that the second heating run displayed a double melting peak around 140 °C, which is different to the single event seen in heating run 1. However, the extent of crystallisation and melting is much smaller in the second heating run, indicating that the crystallisation is a rather slow process. It is difficult to distinguish the overlapping peaks such as those between arrows 3 and 4 as well as 3' and 4'. In fact, the signal at these temperatures might be a mix of endothermic (melting onset) and exothermic (end of the cold crystallisation peak, i.e., crystallisation occurring during the heating run) signals. Finally, it must be noted that the first endotherm in heating run 1 (event 1) was especially difficult to interpret as it was most likely a combination of the T_g (heat capacity related baseline change), enthalpy recovery (also seen in heating run 2 for 1'), solvent/moisture evaporation (as shown by thermogravimetric analysis, see S1) and the start of the cold crystallisation peak (3). Because of this, and because of differences in the appearance of the final melting peak (4) on heating run 1 (due to differences in crystallinity between freeze dried batches), sections 3.1.2 and 3.1.3 of the results section will focus only on differences in heating run 2 for different parameters.

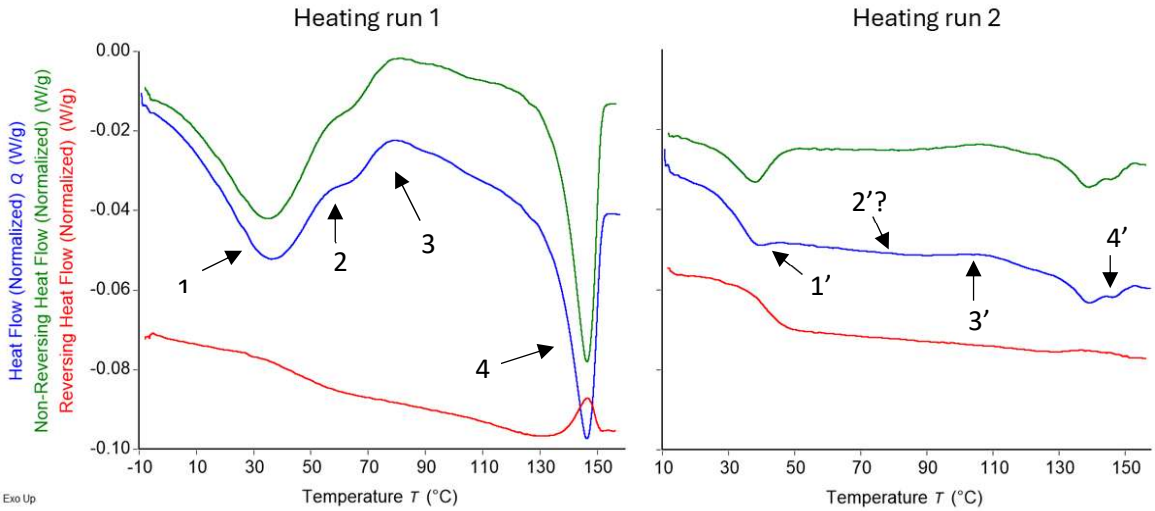

Figure 5. Heating runs 1 and 2 of a PnPrOx 50 kg/mol sample at 2 °C/min and cooled at 47 °C/min between heating runs. Thermal events are linked to solvent/moisture evaporation (heating run 1, 1) Tg (1 and 1'), enthalpy recovery (1 and 1'), start of crystallisation (1), melting (2 and 2'), cold crystallisation (3 and 3'), final melting (4 and 4').

3.2.2 mDSC analysis of PnPrOx 50 kg/mol using different heating and cooling rates

Figure 6 shows the differences between the total heat flows of the second heating run of PnPrOx (50 kg/mol) heated at 1 °C/min and 2 °C/min, respectively. Both were cooled at 47 °C/min. Cold crystallisation in the 1 °C/min heating curve peaked at approximately 95 °C and was much stronger compared to when heated at 2 °C/min for which the peak occurred at 107 °C. A striking difference resided in the different melting behaviour. When the sample was heated more rapidly, two distinct melting peaks were visible (melting one and melting two), where the first melting event seemed more prevalent. On the other hand, when the sample was heated more slowly, the double melting peak disappeared almost entirely, and the first melting event had become a shoulder of the second. The reader can refer to the supplementary information (S6) for other identical thermograms, as all analyses were conducted in triplicate and were reproducible.

375 The sample shown as the green curve in Figure 6 was subjected to a third heating run and subsequently
376 cooled at an average rate of 47 °C/min, which resulted in an identical thermogram when compared to
377 the second heating run (Figure 6, green curve). This sample was then kept at ambient conditions for a
378 week and subsequently re-analyzed with mDSC using a heating rate of 2 °C/min, which is shown as the
379 red curve in Figure 6. The material underwent some structural changes during this period, as the
380 thermograms were different. Notably, the T_g shifted to lower temperatures and a broad endotherm
381 appeared, stretching from right after T_g up to at about 80 °C where the exothermic cold crystallization
382 signal starts. The endotherm likely links to the removal of water, taken up during storage. The presence
383 of water leads to a plasticization effect also explaining why the T_g of the stored sample is considerably
384 reduced compared to when heated right after cooling in DSC. The exothermic peak appears at about
385 the same temperature as in the heating run at 1 °C/min (Figure 6 blue curve), although heating in this
386 case was conducted at 2 °C/min. The earlier cold crystallization in the red curve, compared to in the
387 green, suggests a facilitated nucleation. The latter is tentatively associated with crystal fragments
388 formed during the storage time. Indeed, the water uptake might reduce the T_g by which the mobility
389 increases sufficiently to permit the (slow) creation of crystal fragments. The relevance of nucleating
390 crystal fragments for the cold crystallization characteristics is demonstrated once more in the next
391 section where such fragments are permitted to grow during a slow cooling run instead of isothermally
392 during storage.

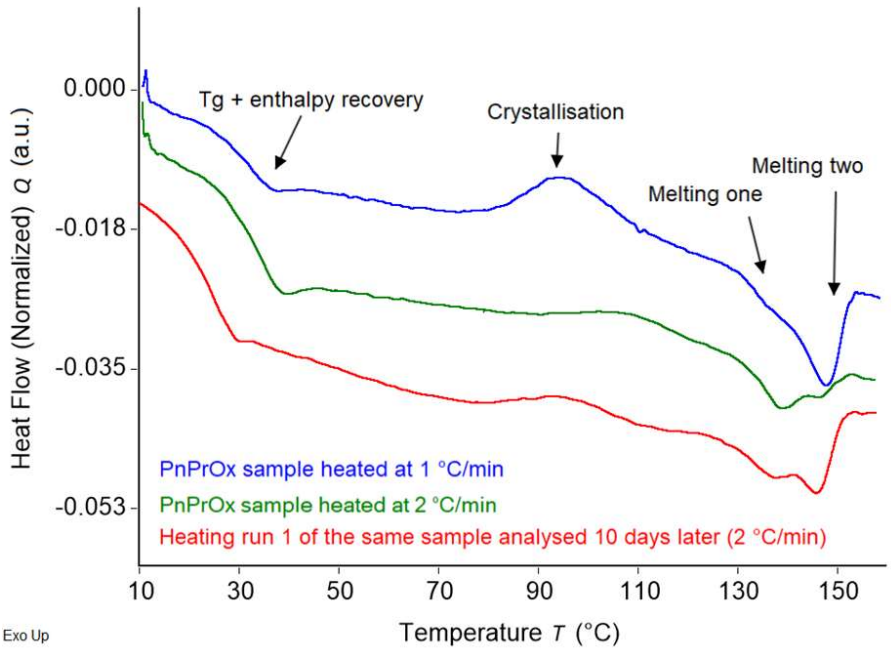

Figure 6. Total heat flow thermograms of heating run 2 of a PnPrOx 50 kg/mol sample heated at 1 °C/min (blue) and at 2°C/min (green). One sample was kept at room temperature in the DSC pan for 10 days and subsequently re-analysed using the same protocol (heating at 2 °C/min). Its first heating run is shown in red. Note that these thermograms were not normalized for

3.2.3 mDSC analysis of PnPrOx 50 kg/mol using different cooling rates

The behaviour of the system was also studied by using different cooling rates. Figure 7 shows another overlay of total heat flows in heating run 2. This time, all the samples were heated at 2 °C/min, but were cooled at 47 °C/min (average rate), at 5 °C/min, and at 2 °C/min, respectively. Replicates not shown here can be found in the supplementary information (S7).

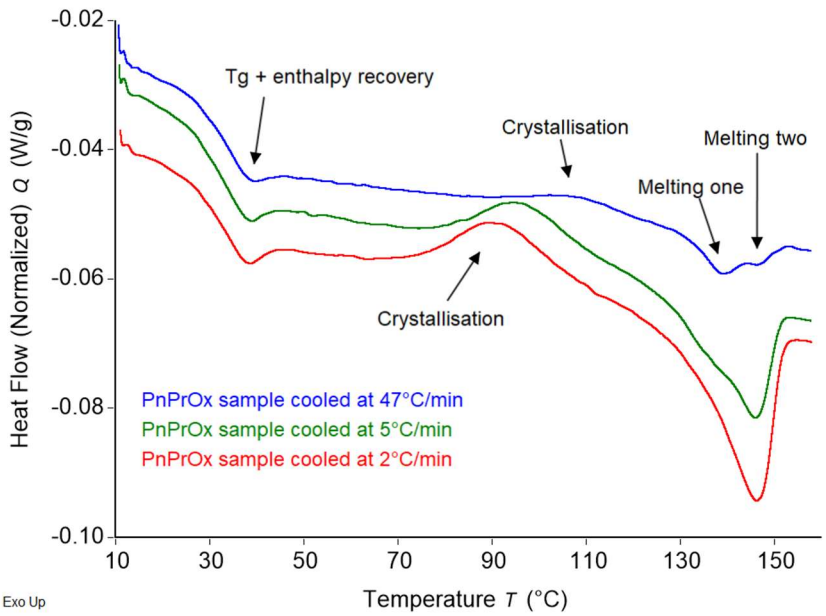

Figure 7. Total heat flow thermograms of heating run two of a PnPrOx 50 kg/mol sample cooled at 47 °C/min (blue), at 5 °C/min (green), and at 2 °C/min (red). The heating rate was 2 °C/min in all cases.

It is clear from Figure 7 that the cooling rate substantially affected the crystallisation behaviour and the corresponding melting peak. When cooled at an average rate of 47 °C/min, the typical double melting peak was obtained. When cooling at 2 °C/min, melting peak one was barely present, and it is best described as the shoulder of melting peak two. Cooling at 5°C/min yielded something in between these two results. Furthermore, the cold crystallisation peak also shifted to lower temperatures when using slower cooling rates.

The explanation for the latter can be found in the cooling runs of the same samples, shown in Figure 8. Some crystallisation occurred during cooling at 5 °C/min, but was more pronounced when cooled at 2 °C/min. This also indicates that crystallisation would certainly have occurred during the conditioning step performed before the SAXS analysis (cooling at 1 °C/min). During the fast cooling at an average rate of 47 °C/min, no crystallisation occurred (see supplementary information, S6). In the previous section, it was shown that slower heating rates also led to a higher contribution of the second melting peak, while this section shows a similar effect for slower cooling rates.

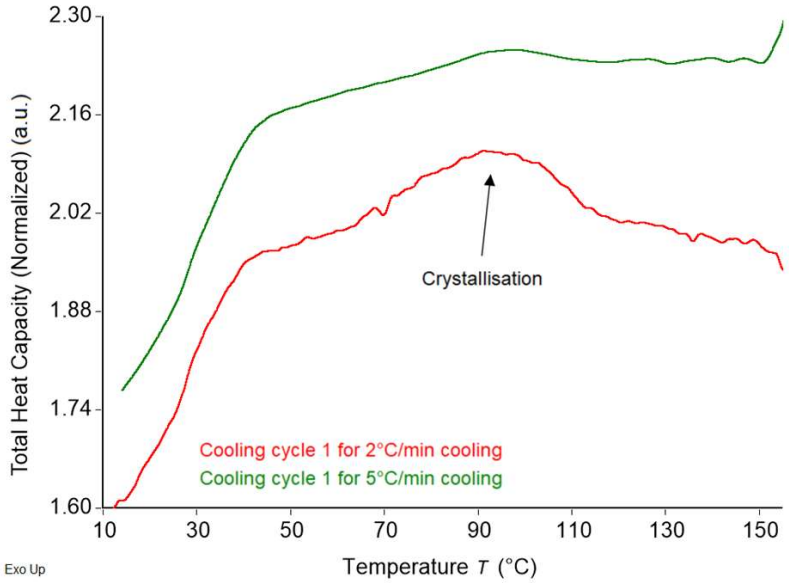

Figure 8. Total heat capacity thermograms of cooling run one of a PnPrOx 50 kg/mol sample cooled at 5 °C/min (green), and at 2 °C/min (red). Total heat capacity was used instead of total heat flow to normalize for the different cooling rates.

3.2.4 Static SAXS and WAXS measurements of PnPrOx 50 kg/mol

The statements made above were corroborated with further structural information. The data above suggest that when the PnPrOx 50 kg/mol sample was cooled slowly, crystallisation occurred during the cooling run. This was also evidenced by the difference in crystallinity detected by the temperature controlled XRPD and synchrotron measurements. The sample was cooled at 1 °C/min before performing the synchrotron measurement, whereas previously melted and rapidly cooled PnPrOx 50 kg/mol was used for the XRPD measurement. A static SAXS/WAXS experiment was performed to see whether this difference could be understood in more detail (Figure 9).

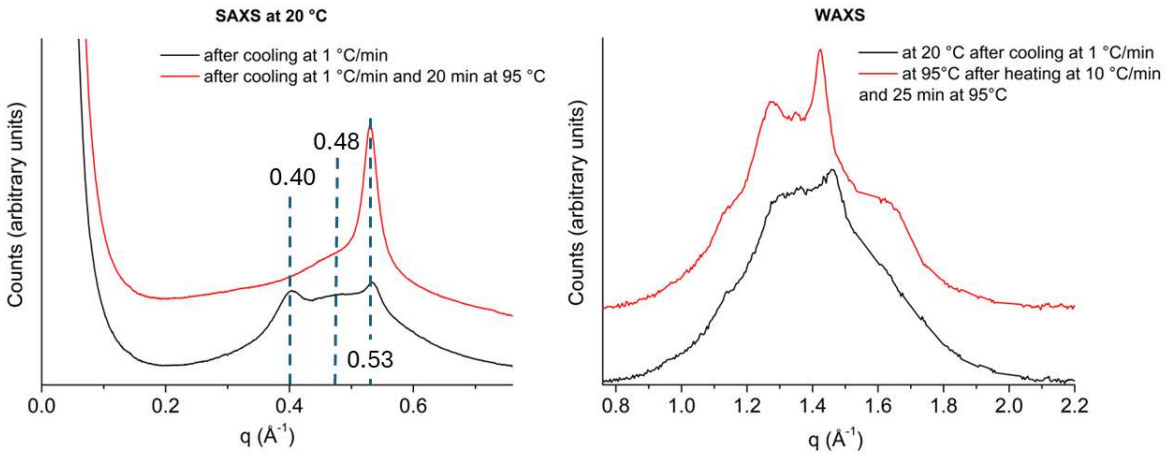

Figure 9. SAXS/WAXS data of PnPrOx 50 kg/mol at 20 °C after cooling at 1 °C/min (black). WAXS data at 95 °C after subsequent heating to 95 °C and 25 min isothermal time (red, right side image). SAXS data at 20 °C after subsequent cooling from 95 °C (red, left side image).

The diffractograms in Figure 9 confirm that a sample that was cooled from the molten state at 1 °C/min was indeed semicrystalline, something that was already evident from the time-resolved WAXS measurement (Figure 4). The peaks around $q = 0.53\ \text{Å}^{-1}$ also correspond to those observed during the XRPD measurement (Figure 3).

In Figure 9, it can also be seen that the crystallinity further increased after an additional 25 min isothermal step at 95 °C. Moreover, significant differences in the SAXS peaks suggest that there might, in fact, be two polymorphic forms present, characterized by the peaks at $q = 0.40\ \text{Å}^{-1}$ (form 1) and $q = 0.53\ \text{Å}^{-1}$ (form 2) respectively. The peak at $q = 0.48\ \text{Å}^{-1}$ is particularly broad and is more likely to be due to an underlying amorphous halo. From this, it can be concluded that form 1 disappears when the sample is heated to 95 °C and does not return. Meanwhile, form 2 grows when annealed at 95 °C. Finally, the peak at $q = 0.48\ \text{Å}^{-1}$ belonging to amorphous material decreases. Therefore, form 1 is metastable and only forms at lower temperatures.

3.2.5 Annealing PnPrOx at 105 °C in the DSC

To further mimic the SAXS/WAXS data, a PnPrOx 50 kg/mol sample was heated to 160 °C to melt all preexisting crystals, cooled down to room temperature at an average rate of 47 °C/min, and then annealed at 105 °C for two hours. This was followed by cooling the sample back to 20 °C at 2 °C/min and subsequently heating it at 1 °C/min, 2 °C/min, or 10 °C/min (Figure 10). The mass normalized heat capacities are shown instead of the total heat flows to avoid large differences in signal magnitude due to the different heating rates. Replicates are shown in the supplementary information (S8).

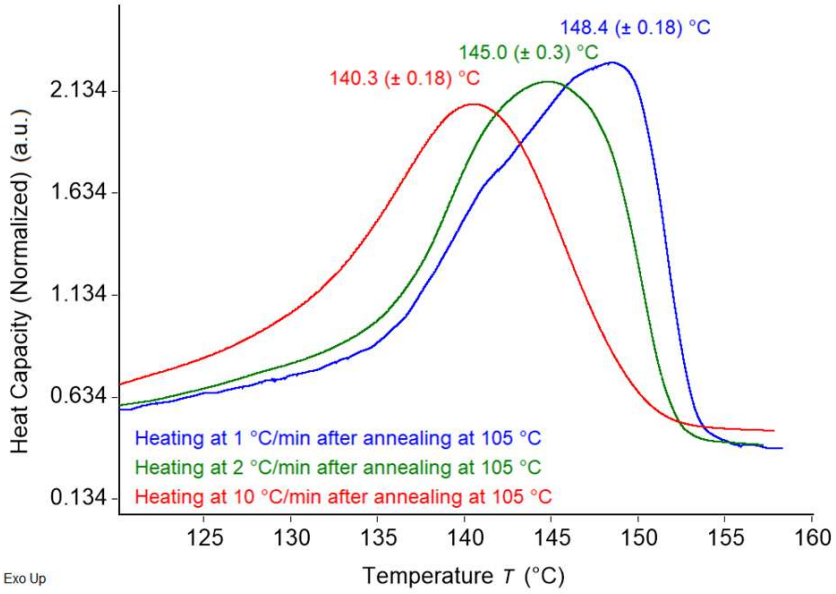

Figure 10. Normalized heat capacity curves of a PnPrOx 50 kg/mol sample annealed at 105 °C and re-heated at different heating rates (1 °C/min in blue, 2 °C/min in green, 10 °C/min in red). The melting peak temperatures are indicated above their respective curves.

As shown in Figure 10, the melting peak temperature decreased with increasing heating rate, whereas the opposite was true for indium (supplementary information, S9). The mDSC instrument was only calibrated for a heating rate of 2 °C/min, but the relevant other heating rates were also applied to an indium reference to identify the deviations (supplementary information, S9). The deviations for PnPrOx were much large compared to indium, and most importantly, the melting peaks shifted to a different direction (indium upward and PnPrOx downward with increasing heating rate).

503 The difference in T_m (peak) was up to 8 °C. This is counterintuitive, as one expects more thermal lag
504 when increasing the heating rate. However, we are not the first to report this, as this deviation was also
505 observed by Oleszko-Torbus *et al.* (10) The deviation can be explained by overlapping recrystallisation
506 and melting phenomena, which will be addressed further in the discussion section.

507 The annealing experiment was also performed for lower molar mass PnPrOx with 11 and 23 kg/mol.
508 First and foremost, these polymers were found to also be semicrystalline despite them being much
509 shorter than the 50 kg/mol PnPrOx. Interestingly, increasing the heating rate also decreased the peak
510 temperature for PnPrOx of these molar masses. For the 11 kg/mol PnPrOx, the melting peak
511 temperatures were 144.9 (± 0.2) °C, 143.0 (± 0.06) °C, and 139.4 (± 0.006) °C for heating rates of 1
512 °C/min, 2 °C/min, and 10 °C/min respectively. For the 23 kg/mol PnPrOx, the melting peak
513 temperatures were 147.6 (± 0.3) °C, 144.9 (± 0.10) °C, and 140.9 (± 0.07) °C for heating rates of 1 °C/min,
514 2 °C/min, and 10 °C/min respectively. The thermograms of these samples are shown in the
515 supplementary information section S10. The melting temperatures show a slight increase with
516 increasing molar mass, demonstrating the presence of slightly more intermolecular interactions due to
517 the longer polymer chains. The fact that increasing the heating rate for lower molar mass PnPrOx has
518 the same effect as for 50 kg/mol PnPrOx demonstrates that the lower molar mass PnPrOx have very
519 similar properties as the 50 kg/mol PnPrOx. Further interpretation of this result is performed in the
520 discussion section.

521 Something else that is clear from the data in Figure 10 is the lack of two distinct melting peaks. When
522 the sample was given enough time to anneal at an elevated temperature, the melting endotherm was
523 much broader. The heating rate now had a much smaller effect on the presence of melting peak one
524 or two, in contrast to the results presented for the different heating and cooling rates. Moreover, there
525 was no indication for crystallisation during heating. This suggests that the material was crystallised to
526 a greater extent after having been annealed under these conditions. The endotherm (melting) that

appeared before the crystallisation peak was also not present (although there might still have been overlapping crystallisation and melting, as described in the discussion section).

To further study the behaviour of the sample after it was annealed, a PnPrOx (50 kg/mol) sample was melted and then flash cooled with liquid nitrogen before storing it in an oven at 60 °C for one week (which is above the T_g). Figure 11 (left) shows the first heating run of the resulting mDSC analysis, while Figure 11 (right) shows the XRPD diffractogram prior to heating. The other mDSC replicates can be found in the supplementary information (S11).

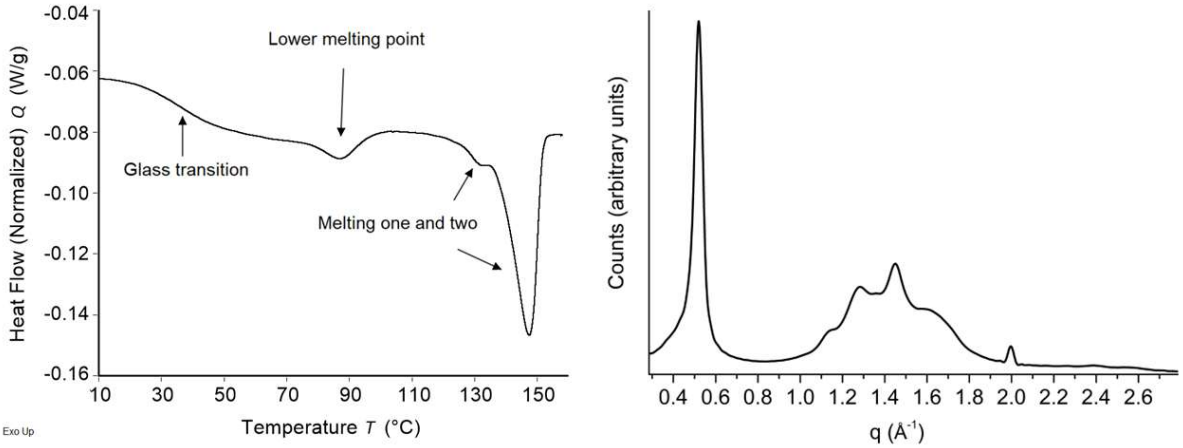

Figure 11. Left: mDSC thermogram showing the total heat flow (blue) of a PnPrOx 50 kg/mol sample annealed at 60 °C for a week and subsequently analyzed (heating run 1). Right: XRPD diffractogram of the same sample.

The sample appears to have been very crystalline, as evidenced by a large endotherm at around 147 °C. What is interesting is that there appears to be another melting endotherm at around 85 °C. There are also significant differences above 95 °C between the thermogram show in Figure 11 and the ones shown in Figure 7 for instance. It is especially clear that the cold crystallisation exotherm is less pronounced, indicating that the material is more crystalline. Interestingly, melting one is still present, indicating that imperfect crystals are still present.

3.3 Crystallisation from aqueous solution of PnPrOx

As mentioned in the introduction, it has been reported for PiPrOx that it crystallizes when an aqueous PiPrOx solution is annealed above its T_{Cp}. Hence, it was interesting to conduct a similar experiment for PnPrOx (50 kg/mol) in the context of this study. When the temperature exceeded the T_{Cp}, the PnPrOx solution did at first become cloudy, but then the polymer formed a precipitate consisting of larger particles that settled out of the solution after several hours. The abovementioned particles remained visible after cooling the solution below the T_{Cp} for several weeks, suggesting that some irreversible transition had occurred.

To confirm that the particles mentioned above were indeed PnPrOx crystals, they were analysed with mDSC as well as XRPD (Figure 12 (left) and (right), respectively). These analyses further confirmed the crystallinity of the sample. The other mDSC replicates can be found in the supplementary information (S12).

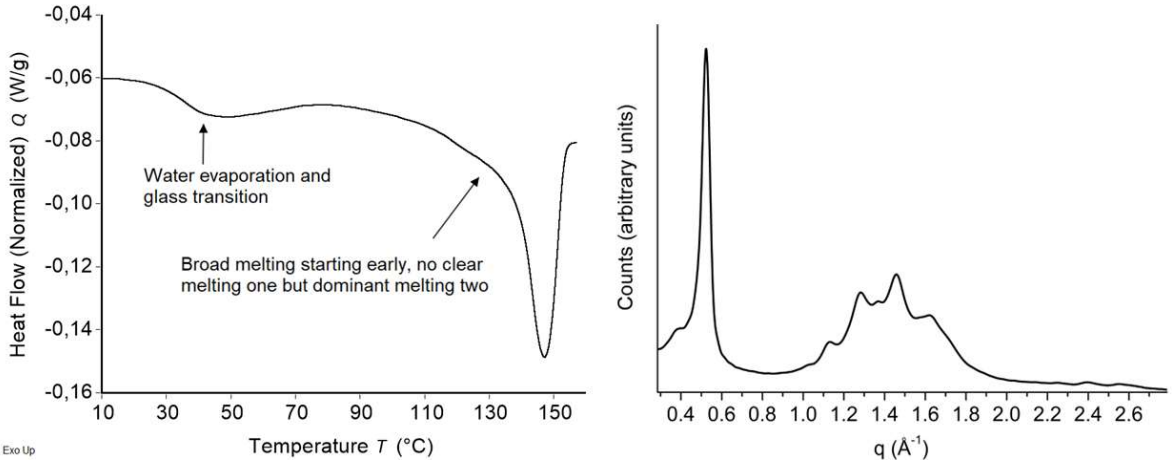

Figure 12. Left: total heat flow (blue), curves of a PnPrOx 50 kg/mol sample that crystallized from aqueous solution. Right: XRPD diffractogram of the same sample.

Aside from the fact that this meant that the T_{Cp} is not reversible for PnPrOx when an aqueous solution was annealed at higher temperatures, but below its T_m, it must be noted that this sample was the most crystalline of all samples analysed, with a melting enthalpy of around 25 J/g. In fact, this value was probably even higher, since the sample was still moist when it was prepared for mDSC analysis. Despite

563 the isotherm that was prepared to remove some of the water, a small water evaporation endotherm
564 (as well as a T_g) remains visible on Figure 12a. Thermogravimetric analysis (see supplementary
565 information S2) indicated a further reduction in mass of 28% m/m between room temperature and 65
566 °C, indicative of the loss of water, meaning that the real melting enthalpy could have been as high as
567 32 J/g. Moreover, as opposed to the sample shown in Figure 11 that was annealed at 60 °C, melting
568 one was no longer clearly present despite the presence of a broad endothermic melting signal starting
569 around 110 °C.

4 Discussion

4.1 Comparison with previous work

The T_m reported for PnPrOx of all molar masses in this work corresponds to previous work from our group, (4) but not to those reported in the Oleszko-Torbus paper. (10) Both papers mention the double melting peak, but at different temperatures. This can be explained by differences in the PnPrOx that was used. Oleszko-Torbus *et al.* used PnPrOx with a number average molar mass of 8.7 kg/mol (Đ = 1.03), while the current study (and that of previous findings from our group (4)) used PnPrOx with a number average molar mass of 50 kg/mol (Đ ≤ 1.25) down to 11 kg/mol (Đ ≤ 1.25). Moreover, Oleszko-Torbus *et al.* used PnPrOx prepared with methyl 4-nitrobenzenesulfonate as initiator and n-propylamine as terminating agent, followed by solvent evaporation without further purification. In contrast, the 50 kg/mol PnPrOx used in this work had a phenyl oxazoline α-group, BF_4^- as counter anion and a hydroxyl ω-group, which was also used directly after solvent evaporation. The lower molar mass PnPrOx used in this work had a methyl α-group, and a hydroxyl ω-group. The difference in M_n partially explains the lower T_m found by Oleszko-Torbus *et al*., but it is possible that end groups as well as the difference in Đ also have an impact on the T_m of the polymers from the work of Oleszko-Torbus *et al*. The trend seen in this work further shows this to be the case, since the T_m did decrease with decreasing molar mass, but only very slightly, further indicating that the end groups might play a more important role.

The differences between the present work and previous work also explain why PnPrOx was found to be fully amorphous in earlier publications, (24) as shorter polymer chains may not crystallize or crystallize very slowly, making crystallisation harder to detect. This being said, differences in heating rate may also play a role, since slower heating promotes cold crystallisation and this manuscript mainly uses a slower heating rate of 2 °C/min. Similarly, for the crystallisation event Oleszko-Torbus *et al.* report no cold crystallisation upon heating for PnPrOx, which is indeed clear from their data. They used

heating rates of 10 °C/min and 2.5 °C/min and did not find cold crystallisation for either heating rate. Previous findings from our group (4) do not explicitly exclude cold crystallisation for PnPrOx, and a cold crystallisation event can in fact be seen in the thermograms at a similar location to the one reported in this paper. This indicates that the presence of a cold crystallisation event during the heating cycle also depends on the chain length. It would be interesting to investigate the relationship between semi-crystallinity and chain length further, not only for PnPrOx, but also for the other PAOx, in future work.

4.2 The shift of melting peaks and the double melting peak

An explanation for the shift of the melting peaks to lower temperatures when the heating rate is higher (Figure 10) can be found in a paper by Schulz *et al.*, who have previously reported this behaviour for polycaprolactone. (41) The authors attribute this behaviour to competing crystallisation and melting events, whereby crystallisation is slower than melting. This means that when a faster heating rate is used, there is less time for (re)crystallisation to happen, resulting in a larger contribution from the melting that also appears at a lower temperature when the heating rate is higher (as seen in Figure 10). This also means that for all heating runs, there is melting after recrystallisation. This happens for the material annealed at 60 °C with the low melting peak (Figure 11), but also in the case of the double melting peak.

The temperature-controlled WAXS experiment, which only required seconds for analysis at a certain temperature, also displayed a shift in T_m with respect to the XRPD experiment, which required two hours for analysis at each temperature. Firstly, as can be seen in Figure 4, the crystal peak intensity decreased (indicating that crystals are melting), while crystal size increased. This hints at the material undergoing reorganizations as the melting occurs. Interestingly, this is also the explanation for the apparent contradiction between Figure 3 (XRPD experiment) and Figure 4 (WAXS experiment). In Figure 3, Bragg peaks were still visible at 150 °C, whereas the crystal intensity was close to zero at 143 °C in Figure 4. This indicates that during the XRPD experiment, the melting was not finished at 150 °C,

whereas it was finished at 143 °C during the faster WAXS experiment. This is most likely the exact same shifting of the melting peak as was seen in the mDSC thermograms, although it could also be partially due to errors in the exact temperature measurement.

Finally, this behaviour can also explain the double melting peak. Neither the WAXS nor XRPD data suggested that the melting peaks still present at higher temperatures belong to different polymorphs. Hence, combining this knowledge with what was stated about the increasing crystal size in Figure 4, it can be concluded that the double melting peak is due to differences in crystal size.

If the different T_m values are to be explained through differences in crystal size (or thickness) and not polymorphism, the explanation for the different T_m is expressed through the Gibbs-Thomson equation:

$$T_m(n) = T_m^{\infty} - \frac{2\sigma_e T_m^{\infty}}{\Delta H_m d_c}.$$

Where T_m is the melting temperature for a microscopic crystal of thickness d_c, $T_m^{\infty}$is the melting temperature of an infinitely large crystal sample, ΔH_m is the melting enthalpy, and σ_e is the surface free energy of polymer chains located at the two surfaces of the crystal (assuming crystal lamellae). (42) This equation shows that if thicker or larger crystals are present, the T_m is closer to that of a macroscopic sample, meaning it is higher. Thus, smaller crystallites result in a larger melting point depression. It is remarkable that no shape scattering was recorded with SAXS when the detector was placed at 3 m from the sample to record q-values starting at $0.006\ \text{Å}^{-1}$. This setup can detect crystals up to 100 nm in size, indicating that PnPrOx crystals exceed this threshold or that the electron density difference between the crystallites and the surrounding amorphous matter is vanishingly low by which they escape the observation.

Something left to explain is the nature of the melting peak at around 85 °C that appeared when an amorphous sample was annealed at 60 °C for a week (Figure 11). Again, the reader is referred to the paper by Schulz *et al.* (41) They also report a small melting peak, T_{m0}, whose presence and location depends on the crystallisation (annealing) temperature. According to the authors, this peak might be

due to very thin, unstable crystalline lamellae (thin crystal sheets) forming at low annealing temperatures that melt earlier than the final T_m. Following this melting event, the material continuously melts and recrystallizes before a final T_m is reached. Based on the data presented here, it is possible that PnPrOx follows similar behaviour.

Finally, it must be noted that 60 °C is apparently not sufficient to only form large crystals, since melting peak one was still present on the corresponding thermogram (Figure 11). However, when PnPrOx crystallized from a sample kept above its T_{Cp}, larger crystals were formed, as demonstrated by a complete lack of melting peak one in Figure 12. Annealing at 105 °C for two hours (Figure 10) results in an intermediate result, where neither melting peak one nor two is clearly present.

Previous studies have found that a change to an all-trans conformation plays an important role in the crystallisation process of PiPrOx when it is kept above its T_{Cp}. (35) Conformation changes might also play a role in forming more perfect crystals when PnPrOx crystallizes from aqueous solution. Further research that can distinguish between conformations would be interesting for PnPrOx as well and could be done using spectroscopy, such as Fourier-transform infrared spectroscopy.

4.3 Overview of the effects observed when using different cooling- and heating rates for mDSC

Table 1 summarizes the data reported for 50 kg/mol PnPrOx in sections 3.1.2 and 3.1.3 and gives some additional insights. It confirms that there are in fact two possible melting peaks, and that the cold crystallisation peak (i.e. the crystallisation peak during heating) tends to shift. The peaks that were observed in an mDSC thermogram depend on the heating and the cooling rate. The (cold) crystallisation and melting enthalpies during heating match very well, irrespective of the adopted heating rate, after the sample had been cooled rapidly at an average rate of 47 °C/min. This suggests that the sample was amorphous and that most of the crystallisation happens during the heating run (i.e., cold

667 crystallisation). On the other hand, when slower cooling was used, there was indeed a discrepancy
668 between the crystallisation and melting enthalpies, demonstrating that part of the crystallisation had
669 already happened during the cooling run.

670 *Table 1. Summary of data generated in the DSC heating experiments for PnPrOx 50 kg/mol involving different heating and*
671 *preceding cooling rates.*

Condition	heating run 2 at 2 °C/min after cooling at maximum rate	heating run 2 at 1 °C/min after cooling at maximum rate
Variables	Means (± standard deviations)	Means (± standard deviations)
Cold crystallisation onset	96 (± 13) °C	83.4 (± 1.5) °C
Cold crystallisation peak	107 (± 3) °C	96.5 (± 0.8) °C
Cold crystallisation enthalpy	2.1 (± 0.15) J/g	7.8 (± 0.6) J/g
Melting onset	131.3 (± 0.3) °C	137.6 (± 0.4) °C
Melting peak (largest)	139.2 (± 0.4) °C	147.8 (± 0.12) °C
Melting enthalpy	2.1 (± 0.05) J/g	7.6 (± 0.6) J/g
Condition	heating run 2 at 2 °C/min after cooling at 2 °C/min	heating run 2 at 2 °C/min after cooling at 5 °C/min
Variables	Means (± standard deviations)	Means (± standard deviations)
Cold crystallisation onset	73.5 (± 0.7) °C	79.2 (± 0.5) °C
Cold crystallisation peak	91.6 (± 0.6) °C	96.4 (± 0.4) °C
Cold crystallisation enthalpy	6.3 (± 0.3) J/g	4.6 (± 0.12) J/g
Melting onset	131.1 (± 0.19) °C	131.4 (± 0.6) °C
Melting peak (largest)	146.1 (± 0.06) °C	146.0 (± 0.12) °C
melting enthalpy	11.1 (± 0.7) J/g	7.3 (± 0.18) J/g

672

673 A more in-depth discussion of Table 1 is possible when keeping the previous sections from the
674 discussion in mind. The differences between different heating and cooling rates expressed in Table 1
675 can be summarized as follows:

676 1. Slower heating or cooling resulted in a larger melting enthalpy

2. Slower heating or cooling resulted in a larger cold crystallisation enthalpy
3. The cold crystallisation peak location was also affected by heating and cooling rates. Slower cooling and heating resulted in a crystallisation peak at a lower temperature.
4. Faster heating or cooling resulted in the melting peak at a lower temperature (139 °C) being more important.
5. Slower heating or cooling resulted in the melting peak at a higher temperature (146 °C) being more important.

The first point is straightforward and is caused by the fact that the sample is given more time to crystallize, resulting in a higher melting enthalpy. The second point can also be explained in a similar way when the slower heating rate is concerned, but it is interesting that the slower cooling rate also affects the cold crystallisation enthalpy during the subsequent heating cycle. This points at more crystals forming during the cooling cycle, which promotes crystal growth during the subsequent heating cycle. This apparently also lowers the temperature required for crystal formation, explaining point 3, which is likely due to easier crystal nucleation and/or growth in presence of crystals.

Finally, section two in the discussion pointed out that the higher T_m corresponded to larger, more perfect crystals. When PnPrOx is given more time to crystallize, it tends to form these more thermodynamically stable crystals. This explains points 4 and 5. Note that this T_m was also more prominent for the sample annealed at 105°C for two hours, for the sample annealed at 60°C for a week, and for the sample that crystallized in aqueous solution due to the irreversible cloud point transition. Another reason the change in the most prominent melting peak might occur is due to the recrystallisation after melting. During the mDSC run, the smaller crystals melt as apparent from the first melting peak, recrystallize, and then melt again in the second melting peak, making the latter more prominent. This phenomenon is more important when a heating rate of 1°C/min is used, since this gives more time for the recrystallisation to occur.

4.4 Polymorphism

The WAXS data from Figure 4 and the data for intermediate angles from Figure 9 both suggest the existence of a second polymorph with a lower T_m. When studying thermograms such as the one shown in Figure 5 (heating run 1) or in Figure 6 and Figure 7, it can be seen that an endotherm might be present that overlaps with the cold crystallisation peak. The exothermic signal in Figure 8 right before the occurrence of vitrification might be the formation of this form. The fact that these crystals only appear in certain circumstances, disappear upon annealing (SAXS data Figure 9) and at much lower temperatures indicates that they are unstable.

None of the mDSC experiments performed here go into much depth regarding this potential polymorph, since this manuscript focuses on explaining the melting and crystallisation events occurring at higher temperatures. It would however be interesting to investigate whether there is another polymorph and whether polymorphism might be present in other PAOx as well. Once more, it must be noted that polymorphism might be related to changes in conformation, as was highlighted above. Further investigations are required to determine this conclusively.

4.5 Relevance for future pharmaceutical applications of PnPrOx

As was mentioned in the introduction, PnProx has already been applied for sustained release matrix systems. These drug delivery systems control drug release by allowing a drug to slowly diffuse out of an insoluble polymer matrix. This is in contrast to an immediate release dosage form, which disintegrates and allows for much faster drug release. Studies on drug release from poly(l-lactic acid) matrices show that a transition of the polymer from the amorphous to the semicrystalline state results in a two-stage release profile. (43,44) Additionally, Mallapragada and Peppas have developed a controlled release system that is entirely based on crystal dissolution. (45)

More recently, dexamethasone release from polycaprolactone matrices was shown to depend on matrix morphology, including semicrystalline properties. (46) It has also been shown that polyethylene oxide crystal morphology and crystal size can significantly impact drug release from a matrix. Moreover, these properties were directly influenced by processing parameters such as injection mold temperature, demonstrating the importance of considering semicrystalline properties in drug formulation development. (47) Hence, to rationally develop a sustained release matrix with PnPrOx, it is not only crucial to know that it is semicrystalline, but also to know that different crystal sizes, degrees of crystallinity, and morphologies or polymorphs can be present.

On a smaller scale, release from a polymer matrix in the case of micro- or nano-sized drug delivery systems seems to be influenced by semicrystalline properties as well. (48,49) This was shown to be the case by Jeong *et al.* for papaverine release from polycaprolactone microspheres. Moreover, the crystallite size was once more shown to be an important factor for drug release from microparticles by Miles *et al.* It is thus crucial to understand the semicrystalline properties of PnPrOx, including the fact that different crystal sizes can exist, for the development of polymeric microparticles with a PnPrOx matrix.

Another potential application mentioned in the introduction was that of amorphous solid dispersions, where a drug is molecularly dispersed in a polymer matrix, mainly to increase its apparent aqueous solubility and dissolution rate. One of the important parameters governing ASD stability and maximum drug loading is solubility of a drug in the polymer. (50) It stands to reason that when a polymer is partially crystalline, it affects drug solubility since only a fraction of the polymer is amorphous and thus available for drug solubilization. Shi *et al.* reported that fully amorphous polymers were better solubility enhancers and were better at inhibiting crystallisation. (51) Zhu *et al.* reported that the semicrystalline nature of polymers such as poly(ethylene glycol) can also influence the distribution of a drug in an ASD. (52) Finally, the semicrystalline nature of a polymer can also lead to practical considerations that can affect ASD performance. In the case of ASDs prepared by hot melt extrusion for instance,

750 semicrystalline polymers might require higher processing temperatures that can affect physical and
751 chemical stability. (53) Hence, it is clear that a good understanding of the semicrystalline properties of
752 PnPrOx is paramount if it were to be used in ASD development.

753

5 Conclusion

The thermal properties of poly(2-*n*-propyl-2-oxazoline) have been investigated using various techniques before, but this study is the first to go a step further in characterizing its thermal properties. First, this study shows that PnPrOx displays much more complex semi-crystalline behaviour than what was previously assumed, possibly also related to the use of defined higher molar mass PnPrOx (11, 23 and 50 kg/mol). Using a combination of X-ray scattering techniques and mDSC, it was proposed that the polymer may exhibit polymorphism, that different crystal sizes lead to different melting peaks, that the sample crystallizes upon heating, that the T_{Cp} can be irreversible under certain conditions, and that crystallisation and melting overlap between 130-150 °C. This behaviour led to several additional observations, such as a shift of the melting peak to lower temperatures when using higher heating rates and an additional melting peak at 85 °C after annealing at 60 °C.

The interpretation of the data presented in this manuscript would not have been possible with mDSC alone. Although it was a useful tool to quickly investigate the behaviour exhibited by the material, the overlapping peaks might lead to the wrong conclusions. It is only by also looking at structural data obtained by the WAXS/SAXS and XRPD experiments that correct conclusions could be drawn.

The results presented in this manuscript elucidate what transitions happen in PnPrOx, but these could also occur in other PAOx. It is essential to conduct more research regarding the fundamental properties of these polymers if we want to apply them rationally in the biomedical field, such as in the formulation of matrix systems, amorphous solid dispersions, nanoparticle drug delivery systems, and so forth. For example, the crystalline properties of PnPrOx and any changes hereof could affect the release kinetics of such formulations and thus be a decisive factor when considering their stability. The results also indicate how PnPrOx reacts upon heating, helping with the future thermal analysis of the material when it is incorporated in more complex formulations.

Acknowledgements

The authors would like to acknowledge Bernard Appeltans's help with XRPD and mDSC experiments, Ali Tigrine and Martin Purino who synthesized the polymers for a previous study and Senne Lauryssen who helped with the experiment involving the sample annealed at 60 °C for a week and the experiment where an aqueous PnPrOx solution was kept above its T_{Cp}. This research was funded through an FWO grant (1SH0S24N). FWO is also acknowledged for supporting the DUBBLE projects (BM26 at the ESRF).

Supporting Information.

- Freeze drying protocol in detail
- Thermogravimetric analysis of freeze dried PnPrOx and the sample crystallized from aqueous solution
- Differences between perforated and unperforated mDSC pan lids and discussion hereof
- Thermograms of PEtOx 50 kg/mol, PEtOx 100 kg/mol, and PsecBuOx 50 kg/mol.
- Thermograms of PnPrOx 11 and 23 kg/mol.
- Replicates of mDSC experiments
- Indium reference analysed using different mDSC parameters

6 References

(1) Sedlacek, O.; Hoogenboom, R. Drug Delivery Systems Based on Poly(2-Oxazoline)s and Poly(2-Oxazine)s. *Adv Ther (Weinh)* **2020**, *3* (1). https://doi.org/10.1002/adtp.201900168.

(2) Jana, S.; Hoogenboom, R. Poly(2-oxazoline)s: A Comprehensive Overview of Polymer Structures and Their Physical Properties—an Update. *Polym Int* **2022**, *71* (8), 935–949. https://doi.org/10.1002/pi.6426.

(3) Glassner, M.; Vergaelen, M.; Hoogenboom, R. Poly(2-oxazoline)s: A Comprehensive Overview of Polymer Structures and Their Physical Properties. *Polym Int* **2018**, *67* (1), 32–45. https://doi.org/10.1002/pi.5457.

(4) Everaerts, M.; Tigrine, A.; de la Rosa, V. R.; Hoogenboom, R.; Adriaensens, P.; Clasen, C.; Van den Mooter, G. Unravelling the Miscibility of Poly(2-Oxazoline)s: A Novel Polymer Class for the Formulation of Amorphous Solid Dispersions. *Molecules* **2020**, *25* (16), 3587. https://doi.org/10.3390/molecules25163587.

(5) Salawi, A. Pharmaceutical Coating and Its Different Approaches, a Review. *Polymers (Basel)* **2022**, *14* (16), 3318. https://doi.org/10.3390/polym14163318.

(6) Verbraeken, B.; Monnery, B. D.; Lava, K.; Hoogenboom, R. The Chemistry of Poly(2-Oxazoline)s. *Eur Polym J* **2017**, *88*, 451–469. https://doi.org/10.1016/j.eurpolymj.2016.11.016.

(7) Monnery, B. D.; Jerca, V. V.; Sedlacek, O.; Verbraeken, B.; Cavill, R.; Hoogenboom, R. Defined High Molar Mass Poly(2-Oxazoline)s. *Angewandte Chemie* **2018**, *130* (47), 15626–15630. https://doi.org/10.1002/ange.201807796.

(8) Hoogenboom, R.; Thijs, H. M. L.; Jochems, M. J. H. C.; Van Lankvelt, B. M.; Fijten, M. W. M.; Schubert, U. S. Tuning the LCST of Poly(2-Oxazoline)s by Varying Composition and Molecular Weight: Alternatives to Poly(N-Isopropylacrylamide)? *Chemical Communications* **2008**, No. 44, 5758–5760. https://doi.org/10.1039/b813140f.

(9) Oleszko-Torbus, N. Recent Advances in Modifications, Properties and Applications of 2-Isopropyl-2-Oxazoline (Co)Polymers. *Polymer Reviews* **2022**, *62* (3), 529–548. https://doi.org/10.1080/15583724.2021.1993252.

(10) Oleszko-Torbus, N.; Wałach, W.; Utrata-Wesołek, A.; Dworak, A. Control of the Crystalline Properties of 2-Isopropyl-2-Oxazoline Copolymers in Condensed State and in Solution Depending on the Composition. *Macromolecules* **2017**, *50* (19), 7636–7645. https://doi.org/10.1021/acs.macromol.7b01639.

(11) Lorson, T.; Lübtow, M. M.; Wegener, E.; Haider, M. S.; Borova, S.; Nahm, D.; Jordan, R.; Sokolski-Papkov, M.; Kabanov, A. V.; Luxenhofer, R. Poly(2-Oxazoline)s Based Biomaterials: A Comprehensive and Critical Update. *Biomaterials* **2018**, *178*, 204–280. https://doi.org/10.1016/j.biomaterials.2018.05.022.

(12) Wilson, P.; Ke, P. C.; Davis, T. P.; Kempe, K. Poly(2-Oxazoline)-Based Micro- and Nanoparticles: A Review. *Eur Polym J* **2017**, *88*, 486–515. https://doi.org/10.1016/j.eurpolymj.2016.09.011.

(13) Hoogenboom, R. The Future of Poly(2-Oxazoline)s. *Eur Polym J* **2022**, *179*. https://doi.org/10.1016/j.eurpolymj.2022.111521.

(14) Keßler, L.; Mishra, R.; Hietala, S.; Lammens, M.; Peltonen, L.; Rades, T.; van Veen, B.; Juppo, A.; Laaksonen, T.; Strachan, C.; Luxenhofer, R. Amorphous Solid Dispersions of Amphiphilic Polymer Excipients and Indomethacin Prepared by Hot Melt Extrusion. *European Journal of Pharmaceutical Sciences* **2025**, *204*, 106960. https://doi.org/10.1016/j.ejps.2024.106960.

(15) Boel, E.; Smeets, A.; Vergaelen, M.; De la Rosa, V. R.; Hoogenboom, R.; Van den Mooter, G. Comparative Study of the Potential of Poly(2-Ethyl-2-Oxazoline) as Carrier in the Formulation of Amorphous Solid Dispersions of Poorly Soluble Drugs. *European Journal of Pharmaceutics and Biopharmaceutics* **2019**, *144*, 79–90. https://doi.org/10.1016/j.ejpb.2019.09.005.

(16) Ramsey, J. D.; Stewart, I. E.; Madden, E. A.; Lim, C.; Hwang, D.; Heise, M. T.; Hickey, A. J.; Kabanov, A. V. Nanoformulated Remdesivir with Extremely Low Content of Poly(2-Oxazoline)-Based Stabilizer for Aerosol Treatment of COVID-19. *Macromol Biosci* **2022**, *22* (8). https://doi.org/10.1002/mabi.202200056.

(17) Samaro, A.; Vergaelen, M.; Purino, M.; Tigrine, A.; de la Rosa, V. R.; Goudarzi, N. M.; Boone, M. N.; Vanhoorne, V.; Hoogenboom, R.; Vervaet, C. Poly(2-Alkyl-2-Oxazoline)s: A Polymer Platform to Sustain the Release from Tablets with a High Drug Loading. *Mater Today Bio* **2022**, *16*. https://doi.org/10.1016/j.mtbio.2022.100414.

(18) Maincent, J.; Williams, R. O. Sustained-Release Amorphous Solid Dispersions. *Drug Delivery and Translational Research*. Springer Verlag December 15, 2018, pp 1714–1725. https://doi.org/10.1007/s13346-018-0494-8.

(19) Schver, G. C. R. M.; Novakovic, J.; Lee, P. I. In Vivo Performance of Amorphous Solid Dispersions Based on Water-Insoluble versus Water-Soluble Carriers: Fenofibrate Case Study. *Int J Pharm* **2025**, *671*. https://doi.org/10.1016/j.ijpharm.2025.125227.

(20) Ryma, M.; Blöhbaum, J.; Singh, R.; Sancho, A.; Matuszak, J.; Cicha, I.; Groll, J. Easy-to-Prepare Coating of Standard Cell Culture Dishes for Cell-Sheet Engineering Using Aqueous Solutions of Poly(2-n-Propyl-Oxazoline). *ACS Biomater Sci Eng* **2019**, *5* (3), 1509–1517. https://doi.org/10.1021/acsbiomaterials.8b01588.

(21) A Study of Weekly Subcutaneous Injections of SER-214 in Subjects With Parkinson's Disease (PD), to Determine the Safety, Tolerability and Pharmacokinetic (PK) Profile of SER-214. *ClinicalTrials.gov identifier: NCT02579473*.

(22) Roozen, E. A.; Lomme, R. M. L. M.; Calon, N. U. B.; Ten Broek, R. P. G.; van Goor, H. Efficacy of a Novel Polyoxazoline-Based Hemostatic Patch in Liver and Spleen Surgery. *World J Emerg Surg* **2023**, *18* (1), 19. https://doi.org/10.1186/s13017-023-00483-x.

(23) Clinical Safety and Performance of GATT-Patch in Open Liver Surgery. *Clinicaltrials.gov identifier: NCT04819945 Updated 19/04/2024*.

(24) Oleszko-Torbus, N.; Utrata-Wesołek, A.; Bochenek, M.; Lipowska-Kur, D.; Dworak, A.; Wałach, W. Thermal and Crystalline Properties of Poly(2-Oxazoline)s. *Polym Chem* **2020**, *11* (1), 15–33. https://doi.org/10.1039/C9PY01316D.

(25) Güner, P. T.; Mikó, A.; Schweinberger, F. F.; Demirel, A. L. Self-Assembled Poly(2-Ethyl-2-Oxazoline) Fibers in Aqueous Solutions. *Polym Chem* **2012**, *3* (2), 322–324. https://doi.org/10.1039/c1py00463h.

(26) Rettler, E. F. J.; Lambermont-Thijs, H. M. L.; Kranenburg, J. M.; Hoogenboom, R.; Unger, M. V.; Siesler, H. W.; Schubert, U. S. Water Uptake of Poly(2-N-Alkyl-2-Oxazoline)s: Influence of Crystallinity and Hydrogen-Bonding on the Mechanical Properties. *J Mater Chem* **2011**, *21* (43), 17331–17337. https://doi.org/10.1039/c1jm12541a.

(27) Jerca, V. V.; Lava, K.; Verbraeken, B.; Hoogenboom, R. Poly(2-Cycloalkyl-2-Oxazoline)s: High Melting Temperature Polymers Solely Based on Debye and Keesom van Der Waals Interactions. *Polym Chem* **2016**, *7* (6), 1309–1322. https://doi.org/10.1039/c5py01755f.

(28) Li, T.; Tang, H.; Wu, P. Molecular Evolution of Poly(2-Isopropyl-2-Oxazoline) Aqueous Solution during the Liquid-Liquid Phase Separation and Phase Transition Process. *Langmuir* **2015**, *31* (24), 6870–6878. https://doi.org/10.1021/acs.langmuir.5b01009.

(29) Sun, S.; Wu, P. Conformational Changes in the Heat-Induced Crystallization of Poly(2-Isopropyl-2-Oxazoline) in the Solid State. *Physical Chemistry Chemical Physics* **2015**, *17* (46), 31084–31092. https://doi.org/10.1039/c5cp05719a.

(30) Meyer, M.; Antonietti, M.; Schlaad, H. Unexpected Thermal Characteristics of Aqueous Solutions of Poly(2-Isopropyl-2-Oxazoline). *Soft Matter* **2007**, *3* (4), 430–431. https://doi.org/10.1039/b616678d.

(31) Litt, M.; Rahl, F.; Roldan, L. G. Polymerization of Cyclic Imino Ethers. VI. X-ray Study of Some Polyaziridines. *Journal of Polymer Science Part A-2: Polymer Physics* **1969**, *7* (3), 463–473. https://doi.org/10.1002/pol.1969.160070302.

(32) Bloksma, M. M.; Weber, C.; Perevyazko, I. Y.; Kuse, A.; Baumgärtel, A.; Vollrath, A.; Hoogenboom, R.; Schubert, U. S. Poly(2-Cyclopropyl-2-Oxazoline): From Rate Acceleration by Cyclopropyl to Thermoresponsive Properties. *Macromolecules* **2011**, *44* (11), 4057–4064. https://doi.org/10.1021/ma200514n.

(33) Hoogenboom, R.; Fijten, M. W. M.; Thijs, H. M. L.; Van Lankvelt, B. M.; Schubert, U. S. Microwave-Assisted Synthesis and Properties of a Series of Poly(2-Alkyl-2-Oxazoline)s. *Des Monomers Polym* **2005**, *8* (6), 659–671. https://doi.org/10.1163/156855505774597704.

(34) Diehl, C.; Dambowsky, I.; Hoogenboom, R.; Schlaad, H. Self-Assembly of Poly(2-Alkyl-2-Oxazoline)s by Crystallization in Ethanol-Water Mixtures below the Upper Critical Solution Temperature. *Macromol Rapid Commun* **2011**, *32* (21), 1753–1758. https://doi.org/10.1002/marc.201100421.

(35) Katsumoto, Y.; Tsuchiizu, A.; Qiu, X.; Winnik, F. M. Dissecting the Mechanism of the Heat-Induced Phase Separation and Crystallization of Poly(2-Isopropyl-2-Oxazoline) in Water through Vibrational Spectroscopy and Molecular Orbital Calculations. *Macromolecules* **2012**, *45* (8), 3531–3541. https://doi.org/10.1021/ma300252e.

(36) Nemati Mahand, S.; Aliakbarzadeh, S.; Moghaddam, A.; Salehi Moghaddam, A.; Kruppke, B.; Nasrollahzadeh, M.; Khonakdar, H. A. Polyoxazoline: A Review Article from Polymerization to Smart Behaviors and Biomedical Applications. *Eur Polym J* **2022**, *178*, 111484. https://doi.org/10.1016/j.eurpolymj.2022.111484.

(37) Park, J. S.; Kataoka, K. Comprehensive and Accurate Control of Thermosensitivity of Poly(2-Alkyl-2-Oxazoline)s via Well-Defined Gradient or Random Copolymerization. *Macromolecules* **2007**, *40* (10), 3599–3609. https://doi.org/10.1021/ma0701181.

(38) Gommes, C. J.; Goderis, B. CONEX , a Program for Angular Calibration and Averaging of Two-Dimensional Powder Scattering Patterns. *J Appl Crystallogr* **2010**, *43* (2), 352–355. https://doi.org/10.1107/S0021889810001937.

(39) Hubbard, C. R.; Swanson, H. E.; Mauer, F. A. *A Silicon Powder Diffraction Standard Reference Material*; 1975; Vol. 8.

(40) Demirel, A. L.; Tatar Güner, P.; Verbraeken, B.; Schlaad, H.; Schubert, U. S.; Hoogenboom, R. Revisiting the Crystallization of Poly(2-Alkyl-2-Oxazoline)s. *J Polym Sci B Polym Phys* **2016**, *54* (7), 721–729. https://doi.org/10.1002/polb.23967.

(41) Schulz, M.; Seidlitz, A.; Petzold, A.; Thurn-Albrecht, T. The Effect of Intracrystalline Chain Dynamics on Melting and Reorganization during Heating in Semicrystalline Polymers. *Polymer (Guildf)* **2020**, *196*. https://doi.org/10.1016/j.polymer.2020.122441.

(42) Gert Strobl. *The Physics of Polymers*; Springer Berlin Heidelberg: Berlin, Heidelberg, 2007. https://doi.org/10.1007/978-3-540-68411-4.

(43) Miyajima, M.; Koshika, A.; Okada, ichi; Ikeda, M.; Nishimura, K. *Effect of Polymer Crystallinity on Papaverine Release from Poly (L-Lactic Acid) Matrix*; 1997; Vol. 49.

(44) Miyajima, M.; Koshika, A.; Okada, ichi; Ikeda, M. *Effect of Polymer / Basic Drug Interactions on the Two-Stage Diffusion-Controlled Release from a Poly(L-Lactic Acid) Matrix*; 1999; Vol. 61. www.elsevier.com/locate/jconrel.

(45) Mallapragada, S. K.; Peppas, N. A. *Crystal Dissolution-Controlled Release Systems: I. Physical Characteristics and Modeling Analysis*; 1997; Vol. 45.

(46) Samavedi, S.; Joy, N. Identifying Specific Combinations of Matrix Properties That Promote Controlled and Sustained Release of a Hydrophobic Drug from Electrospun Meshes. *ACS Omega* **2020**, *5* (26), 15865–15876. https://doi.org/10.1021/acsomega.0c00954.

(47) Van Renterghem, J.; Dhondt, H.; Verstraete, G.; De Bruyne, M.; Vervaet, C.; De Beer, T. The Impact of the Injection Mold Temperature upon Polymer Crystallization and Resulting Drug Release from Immediate and Sustained Release Tablets. *Int J Pharm* **2018**, *541* (1–2), 108–116. https://doi.org/10.1016/j.ijpharm.2018.01.053.

(48) Kamaly, N.; Yameen, B.; Wu, J.; Farokhzad, O. C. Degradable Controlled-Release Polymers and Polymeric Nanoparticles: Mechanisms of Controlling Drug Release. *Chemical Reviews*. American Chemical Society February 24, 2016, pp 2602–2663. https://doi.org/10.1021/acs.chemrev.5b00346.

(49) Bikiaris, D.; Karavelidis; Karavas; Giliopoulos; Papadimitriou. Evaluating the Effects of Crystallinity in New Biocompatible Polyester Nanocarriers on Drug Release Behavior. *Int J Nanomedicine* **2011**, 3021. https://doi.org/10.2147/ijn.s26016.

(50) Shi, Q.; Chen, H.; Wang, Y.; Wang, R.; Xu, J.; Zhang, C. Amorphous Solid Dispersions: Role of the Polymer and Its Importance in Physical Stability and In Vitro Performance. *Pharmaceutics*. MDPI August 1, 2022. https://doi.org/10.3390/pharmaceutics14081747.

(51) Shi, N. Q.; Lei, Y. S.; Song, L. M.; Yao, J.; Zhang, X. B.; Wang, X. L. Impact of Amorphous and Semicrystalline Polymers on the Dissolution and Crystallization Inhibition of Pioglitazone Solid Dispersions. *Powder Technol* **2013**, *247*, 211–221. https://doi.org/10.1016/j.powtec.2013.06.039.

(52) Zhu, Q.; Taylor, L. S.; Harris, M. T. Evaluation of the Microstructure of Semicrystalline Solid Dispersions. *Mol Pharm* **2010**, *7* (4), 1291–1300. https://doi.org/10.1021/mp1000907.

(53) Huang, S.; Williams, R. O. Effects of the Preparation Process on the Properties of Amorphous Solid Dispersions. *AAPS PharmSciTech*. Springer New York LLC July 1, 2018, pp 1971–1984. https://doi.org/10.1208/s12249-017-0861-7.